Structure and Interaction with Membrane Model Systems of a Peptide Derived from the Major Epitope Region of HIV Protein gp41: Implications on Viral Fusion Mechanism†

Lellys M. Contreras,‡ Francisco J. Aranda,§ Francisco Gavilanes,|| José M. González-Ros,‡ and José Villalaín*,‡

Centro de Biología Molecular y Celular, Universidad "Miguel Hernández", E-03206 Elche, Spain, Departamento de Bioquímica y Biología Molecular, Universidad de Murcia, E-30100 Murcia, Spain, and Departamento de Bioquímica, Facultad de Química, Universidad Complutense, E-28040 Madrid, Spain

Received November 13, 2000

ABSTRACT: The HIV-1 gp41 envelope protein mediates entry of the virus into the target cell by promoting membrane fusion. With a view toward possible new insights into viral fusion mechanisms, we have investigated by infrared, fluorescence, and nuclear magnetic resonance spectroscopies and calorimetry a fragment of 19 amino acids corresponding to the immunodominant region of the gp41 ectodomain, a highly conserved sequence and major epitope. Information on the structure of the peptide both in solution and in the presence of model membranes, its incorporation and location in the phospholipid bilayer, and the modulation of the phase behavior of the membrane has been gathered. Here we demonstrate that the peptide binds and interacts with negatively charged phospholipids, changes its conformation in the presence of a membraneous medium, and induces leakage of vesicle contents as well as a new phospholipid phase. These characteristics might be important for the formation of the fusion-active gp41 core structure, promoting the close apposition of the two viral and target-cell membranes and therefore provoking fusion.

The human immunodeficiency virus (HIV)[1] is the causative agent of the acquired immunodeficiency syndrome (AIDS), which acts by infecting and destroying the $CD4^+$ lymphocytes of the host organism (*1*). Membrane attachment and fusion are the first steps in the cellular infection process, but the molecular mechanisms of such processes have not been satisfactorily elucidated. The HIV envelope glycoprotein, formed by two noncovalently associated subunits, the surface subunit gp120 and the transmembrane subunit gp41, plays a critical role in the life cycle and biology of the virus. For the fusion and mixing of the viral and cellular contents to occur, gp41 must undergo a complex conformational change apparently triggered by the attachment of gp120 to the receptor on the cell surface (*2*). It has been proposed that, after gp120 binding to the CD4 and chemokine receptor of the target cell, there is a loss of the gp120 protein, enabling a reorientation of gp41 which undergoes a conformational transition, changing its nonfusogenic state to its fusion-active one and leading to the insertion of the fusogenic peptide into the cellular membrane and the ensuing membrane fusion (*3*).

Although most of the therapeutical strategies against HIV are focused to inhibit both the reverse transcriptase and protease enzymes, the inhibition of the membrane fusion by direct action on the gp120/gp41 complex (*4*) is nowadays increasing in importance as an additional approach. The gp41 sequence is highly conserved and contains several characteristic features within its sequence as shown in Figure 1. It consists of an N-terminal ectodomain containing the fusogenic peptide, a transmembrane domain, and a C-terminal intraviral segment, besides a major immunodominant region with several epitopes essential for its activity (*5*). The crystal structure of a gp41 ectodomain core in its fusion-active state consists of a six-helix bundle in which a N-terminal trimeric coiled-coil is surrounded by three C-terminal outer helices in an antiparallel orientation and the central part of it formed by a leucine zipper-like repeat sequence (*6*, *7*). The helical-bundle molecule should be required to break the energy barrier for the fusion of the two membranes, an energetically unfavorable process, implying a direct interaction with the lipid membranes (*8*, *9*).

To study the mechanism by which different gp41 derived peptides could modulate virus−cell fusion, different structural and functional studies with synthetic peptides, both in solution and in the presence of phospholipid model membranes, have been performed (*10*−*14*). Membrane-associated peptides often show a remarkable structural behavior, and different experimental conditions can affect both their

† This work has been supported by Grant PM98-0100 from DGESIC, Spain (to J.V.).

* To whom correspondence should be addressed: Dr. José Villalaín, Centro de Biología Molecular y Celular, Universidad "Miguel Hernández", E-03206 Elche-Alicante, Spain. Telephone: +34-966658 762, Fax: +34-966658758, E-mail: boullon@umh.es.

‡ Centro de Biología Molecular y Celular.

§ Universidad de Murcia.

|| Universidad Complutense de Madrid.

[1] Abbreviations: $\Delta\sigma$, chemical shift anisotropy; 2D, two-dimensional; AIDS, acquired immunodeficiency syndrome; ANTS, 8-aminonaphthalene-1,3,6-trisulfonic acid; DMPA, 1,2-dimyristoylphosphatidic acid; DMPC, 1,2-dimyristoylphosphatidylcholine; DMPS, 1,2-dimyristoylphosphatidylserine; DPH, 1,6-diphenyl-1,3,5-hexatriene; DPX, *p*-xylene-bis-pyridinium bromide; HIV, human immunodeficiency virus; LUV, large unilamellar vesicles; MLV, multilamellar vesicles; NBD-PE, *N*-[7-nitro-2-1,3-benzoxadiazol-1-yl]-dipalmitoylphosphatidyethanolamine; ^{31}P NMR, ^{31}P nuclear magnetic resonance; RhB-PE *N*-(lissamino rhodamine B sulfonyl)-dimyristoylphosphatidyethanolamine; TMA-DPH1-(4-trimethylammoniumphenyl)-6-phenyl-1,3,5-hexatriene.

10.1021/bi002613u CCC: $20.00
Published on Web 02/10/2001

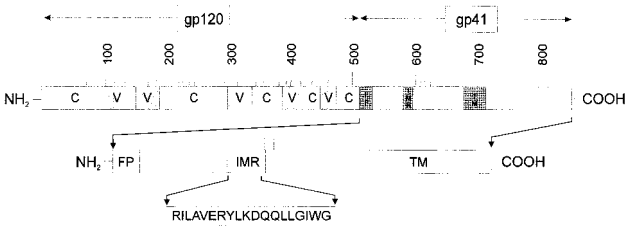

FIGURE 1: A schematic diagram of HIV-1 Env showing the important functional regions in the upper diagram. Hypervariable and conserved regions are indicated as V and C, respectively, and the fusion peptide (FP), the immunodominant region (IMR) and the transmembrane (TM) region are also indicated. In the lower diagram, the gp41 sequence diagram is indicated, showing the location of the sequence of the peptide studied in this work.

conformation and activity. For example, some fusion peptides require an α-helical conformation to be functional (*15*), but also *β*-sheet structures have been proposed to be the active form (*16*). Nevertheless, fusion is also dependent on the specific type of phospholipid used in the model membrane (*16*, *17*). Interestingly, the biologically active fusogenic state appears to involve also oligomeric forms (*11*, *15*).

Here we investigate a peptide comprising a 19-amino acid sequence of the conserved immunodominant region of the gp41 ectodomain, analogous to residues 579−597 of the HXB2R strain (Figure 1). Peptides of this highly conserved region have a strong antiviral activity (*2*), and they are recognized by antibodies from nearly all AIDS patients (*18*). This peptide also includes the terminal sequence of an extended amphipathic α-helix containing a leucine zipper-like region, being suggested that this motif is responsible for the oligomerization of the transmembrane protein, forming a coiled-coil structure (*19*). Moreover, it has been shown that different peptides corresponding to this region show membrane binding (*13*, *19*), and therefore the interaction of this domain with the target cell membrane may be of key importance in the viral fusion mechanism. It is the purpose of the present work to study this gp41 ectodomain fragment both in aqueous solution and in the presence of different membrane model systems composed of a zwitterionic phospholipid, dimyristoylphosphatidylcholine (DMPC), and the negatively charged phospholipids dimyristoylphosphatidic acid (DMPA) and dimyristoylphosphatidylserine (DMPS). Although usually a small amount of phosphatidic acid is present in biomembranes, this phospholipid is believed to play a number of important roles in biological function. Infrared, fluorescence, and nuclear magnetic resonance spectroscopies as well as calorimetry are particularly suited and have been used to obtain structural information on the gp41 fragment when bound to the membrane, to evaluate its incorporation and location in the membrane model systems, and to study its effect on the integrity and phase behavior of the membrane. Our results suggest that this gp41 fragment interacts with negatively charged phospholipids, changes its conformation when bound to the membrane, and induces leakage of vesicle contents and therefore might have a role in the conformational change of the gp41 subunit and subsequent fusion activation.

MATERIALS AND METHODS

Materials. The HIV envelope protein gp41 fragment (Arg−Ile−Leu−Ala−Val−Glu−Arg−Tyr−Leu−Lys−Asp−Gln−Gln−Leu−Leu−Gly−Ile−Trp−Gly) corresponding to amino acids 579−597 from strain HXB2R was synthesized as a C-terminal amide on an automatic multiple synthesizer (AMS 422, Abimed, Lanfengeld, Germany) using a solid-phase procedure and standard Fmoc-chemistry (*20*). The peptide was purified by reverse-phase HPLC to better than 95% purity, and their composition and molecular mass were confirmed by amino acid analysis and mass spectroscopy. Since trifluoroacetate has a strong infrared absorbance at approximately 1673 cm^{-1}, which interferes with the characterization of the peptide Amide I band (*21*), residual trifluoroacetic acid used both in the peptide synthesis and in the HPLC mobile phase was removed by several lyophilization-solubilization cycles in 10 mM HCl (*22*). Lysophosphatidylcholine, cholesterol (Chol), 1,2-dimyristoylphosphatidylcholine (DMPC), 1,2-dimyristoylphosphatidylserine (DMPS), and 1,2-dimyristoylphosphatidic acid (DMPA) were obtained from Avanti Polar Lipids (Birmingham, AL). *N*-(lissamino rhodamine B sulfonyl)-dimyristoylphosphatidyethanolamine (RhB-PE), *N*-[7-nitro-2-1,3-benzoxadiazol-1-yl]-dipalmitoylphosphatidyethanolamine (NBD-PE), 8-aminonaphthalene-1,3,6-trisulfonic acid (ANTS), *p*-xylene-bis-pyridiniumbromide (DPX), 1,6-diphenyl-1,3,5-hexatriene (DPH), and 1-(4-trimethylammoniumphenyl)-6-phenyl-1,3,5-hexatriene (TMA-DPH) were obtained from Molecular Probes (Eugene, OR). Deuterium oxide (99.9% by atom), Triton X-100, EGTA, Hepes, DCl, and KOD were purchased from Sigma (St. Louis, MO). All other chemicals were commercial samples of the highest purity available. Water was twice distilled and deionized in a Millipore system (Millipore, Madrid).

Sample Preparation. Aliquots containing the appropriate amount of lipid in chloroform/methanol (1:1, v/v) were placed in a test tube, the solvents removed by evaporation under a stream of O_2-free nitrogen, and finally, traces of solvents were eliminated under vacuum in the dark for more than 3 h. A preweighed amount of freeze-dried peptide was suspended by addition of an appropriate volume of 20 mM Hepes, 50 mM NaCl, 0.1 mM EDTA, pH 7.4 buffer (either D_2O or H_2O, see below) to give a final concentration of 66 mM. The peptide solution was then added to the tube containing the dried lipid to obtain a final lipid/peptide mole ratio of either 25:1 or 10:1, and the suspension was vortexed at about 5 °C above the transition temperature of the phospholipid to obtain multilamellar vesicles (MLV). The mixture was freezed/thawed twice to ensure complete homogenization of the sample and maximization of contacts between the peptide and the phospholipid and then incubated for 10 min at 55 °C with occasional vortexing. The freeze/thaw cycle was repeated again and the suspension was then centrifuged at 15000 rpm for 15 min to remove the peptide that was not bound to the phospholipid in the membrane. The freeze/thaw, incubation at 55 °C, and centrifugation steps were repeated once more to remove the unbound peptide. The pellet was resuspended in either D_2O or H_2O buffer and used for the measurements.

For fluorescence polarization experiments using either DPH or TMA-DPH, MLV containing both peptide and phospholipid were used. A few microliters of a stock solution of DPH or TMA-DPH at a concentration of 5×10^{-4} M in *N*,*N*′-dimethylformamide were added to the mixture of the MLV suspension and then incubated at 55 °C for 60 min.

In all cases, the lipid/peptide molar ratio was 25:1 and the fluorescence probes/lipid molar ratio was 1:750. When small unilamellar vesicles (SUV) were required for certain fluorescence measurements, MLV were obtained as described above using H_2O buffer, except that no peptide was present. The lipid suspension was freeze/thawed five times to ensure complete hydration and mixing of the phospholipids, and the resulting multilamellar suspension was sonicated with a Branson 250 sonifier (40W) equipped with a microtip until the suspension became completely transparent. Every 30 s, the samples were cooled for 90 s in ice to prevent overheating of the solution. The titanium particles released from the tip were removed by centrifugation at 15 000 rpm at room temperature for 15 min. A small aliquot from this suspension was added to a solution containing a known amount of peptide to give a final and constant peptide concentration (about 1.25 μM). Fluorescence data were obtained immediately afterward as a function of the lipid/peptide molar ratio.

Large unilamellar vesicles (LUV) liposomes were used to study vesicle aggregation, lipid mixing, and leakage. LUV were prepared by the extrusion method (*23*) using polycarbonate filters with a pore size of 0.1 μm (Nuclepore, Pleasanton, California) using 10 mM HEPES, 200 mM NaCl, pH 7.4, buffer. At high concentrations (i.e., inside LUV liposomes), ANTS and DPX form a low fluorescence complex. Breakdown of the vesicle membrane leads to contents leakage, complex decomposition, and high ANTS fluorescence. Thus, buffer used for preparing LUV liposomes for assays of vesicle leakage contained in addition 25 mM ANTS and 90 mM DPX. Nonencapsulated fluorescent probes were separated from the vesicle suspension through a Sephadex G-75 filtration column (Pharmacia, Uppsala, Sweden) eluted with buffer.

The phospholipid and peptide concentrations were measured by methods described previously (*24*, *25*).

Infrared Spectroscopy. For the infrared measurements, MLVs were resuspended in approximately 50 μL of D_2O buffer. Pellets were placed between two CaF_2 windows separated by 50 μm Teflon spacers and transferred to a Harrick Ossining demountable cell. Fourier transform infrared spectra were obtained in a Nicolet 520 Fourier transform infrared spectrometer equipped with a deuterated triglycine sulfate detector. Each spectrum was obtained by collecting 250 interferograms with a nominal resolution of 2 cm^{-1} and triangular apodization using a sample shuttle accessory to average background spectra between sample spectra over the same time period. The spectrometer was continuously purged with dry air at a dew point of −40 °C to remove atmospheric water vapor from the bands of interest. Samples containing DMPA were equilibrated at 25 °C for at least 25 min before acquisition, whereas samples containing DMPC were equilibrated at 10 °C for the same length of time. An external bath circulator, connected to the infrared spectrometer, controlled the sample temperature.

Subtraction of buffer spectra taken at the same temperature as the samples was performed interactively using either GRAMS/32 or Spectra-Calc (Galactic Industries, Salem, MA) as described previously (*26*). Frequencies at the center of gravity, when necessary, were measured by taking the top 10 points of each specific band and fitted to a Gaussian band. Band-narrowing strategies were applied to resolve the component bands in the amide I′ region. Second-derivative spectra were calculated over a 15-data point range. Fourier self-deconvolution (*27*) of the subtracted spectra was carried out using a Lorentzian shape and a triangular apodization with a resolution enhancement parameter, *K*, of 2.2, which is lower than log(signal/noise) (*28*) and a full width at half-height of 18 cm^{-1}. These parameters assumed that the spectra were not over-deconvolved as was evidenced by the absence of negative side lobes. The number and position of the component bands were obtained through both deconvolution and derivation, being the initial bandwidths estimated from the derivative spectra. Protein secondary structure elements were quantified from curve-fitting analysis by band decomposition of the original amide I′ band after spectral smoothing using the same software stated above (*29*).

To obtain two-dimensional infrared correlation spectra and to detect dynamical spectral variations induced by temperature on the secondary structure of the gp41 fragment and on the phospholipid, we have obtained two-dimensional synchronous, $\Phi(\nu_1,\nu_2)$ and asynchronous (disrelation), $\Delta(\nu_1,\nu_2)$, spectra, as defined by

$$\Phi(\nu_1,\nu_2) = \frac{1}{(N-1)}\sum_{i=1}^{N} y(\nu_1,t_i)y(\nu_2,t_i)$$

and

$$\Delta(\nu_1,\nu_2) = \sqrt{\frac{1}{(N-1)}\sum_{i=1}^{N}\sum_{j>i}^{N}\{y(\nu_1,t_i)y(\nu_2,t_j) - y(\nu_1,t_j)y(\nu_2,t_i)\}^2}$$

as it has been described before (*30*). Correlation calculations have been done over the 3050−1350 cm^{-1} spectral region. Calculations were done with the use of Mathcad for Windows software.

Differential Scanning Calorimetry. Differential scanning calorimetry was performed in a high-resolution Microcal MC-2 calorimeter (Microcal Inc., Northampton, MA), equipped with a digital interface and data adquisition utility for automatic data collection. Differences in the heat capacity between the sample and the reference cell were obtained by raising the temperature at a constant rate of 60 °C/h over a temperature range of 15−80 °C. The excess heat capacity functions were obtained after baseline subtraction and correction of the instrument time response. Unless otherwise stated, the second scan was used for transition and enthalpy calculations.

Fluorescence Measurements. Steady-state fluorescence measurements were carried out using a SLM 8000C spectrofluorometer with a 400 W Xe lamp, double emission monochromator, and Glan-Thompson polarizers. Correction of excitation and emission spectra was performed using a Rhodamine B quantum corner solution and a standard lamp. Typical spectral bandwidths were 4 nm for excitation and 2 nm for emission. All fluorescence studies were carried using 5 × 5 mm quartz cuvettes. The excitation and emission wavelength was 290 and 354 nm when observing the peptide fluorescence and 360/362 and 425/450 nm when observing the DPH/TMA-DPH fluorescence. All the data were corrected for background intensities and progressive dilution. Emission spectra were not corrected for the photomultiplier

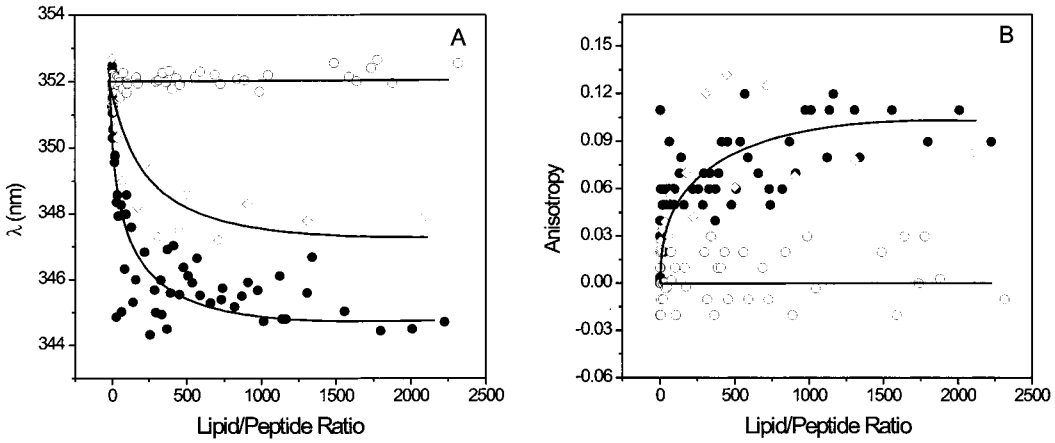

FIGURE 2: Emission maximum (A) and fluorescence anisotropy (B) of the gp41 fragment in the presence of increasing concentrations of small unilamellar vesicles composed of DMPA (●), DMPC/DMPA/Chol at a molar ratio of 50:35:15 (◊), and DMPC (○). The lines connecting the experimental data are merely guides to the eye.

wavelength dependence. Fluorescence anisotropies were determined according to the following equation (*31*),

$$r = \frac{I_{VV} - GI_{VH}}{I_{VV} + 2GI_{VH}}$$

where I_{VV} and I_{VH} are the fluorescence intensities and the subscripts indicate the vertical (V) or horizontal (H) orientations of the excitation and emission Glan−Thompson polarizers. The instrumental factor G ($G = I_{HV}/I_{HH}$) was determined by measuring the polarized components of fluorescence of the peptide or probes with horizontally polarized excitation. The partition coefficient between the lipid and the aqueous phases, K_p, was determined by the change in the spectroscopic parameters of the peptide when bound to the phospholipid as described previously (*13*).

Vesicle aggregation was followed as an increase in light scattering at 90° with both monochromators of the spectrofluorometer at 520 nm. Leakage was assayed by treating the probe-loaded liposomes (final lipid concentration, 0.1 mM) with the appropriate amounts of peptide in a fluorometer cuvette stabilized at different temperatures. Changes in fluorescence intensity were recorded with excitation and emission wavelengths set at 350 and 510 nm, respectively. One hundred percent release was achieved by adding to the cuvette Triton X-100 to a final concentration of 0.1% (w/w). Leakage was quantified on a percentage basis according to the equation,

$$\% \text{ release} = \left(\frac{F_f - F_0}{F_{100} - F_0}\right) \times 100$$

F_f is the equilibrium value of fluorescence after peptide addition, F_0 is the initial fluorescence of the vesicle suspension, and F_{100} is the fluorescence value after addition of Triton X-100. Peptide induced vesicle lipid mixing was measured as described in ref *32* using LUV liposomes. The concentration of each of the fluorescent probes, NBD-PE and RhB-PE, was 0.6%. Labeled and unlabeled LUV vesicles in a proportion 1:4 were placed in a fluorometter cuvette at a final lipid concentration of 0.1 mM and treated with the appropriate amounts of peptide. Fluorescence was measured with the excitation and emission wavelengths set at 460 and 536 nm, respectively, and a 515 cutoff filter was placed between the sample and the photomultiplier.

^{31}P-Nuclear Magnetic Resonance. The samples for ^{31}P NMR were prepared as stated above for the infrared measurements except that H_2O instead of D_2O was used. The suspensions were placed into conventional 5 mm NMR tubes, and ^{31}P NMR spectra were obtained in the Fourier transform mode in a Varian Unity 300 spectrometer. All chemical shift values are quoted in parts per million (ppm) with reference to pure lysophosphatidylcholine micelles (0 ppm), positive values referring to low-field shifts. All spectra were obtained in the presence of a gated-broad band decoupling (10 W input power during acquisition time), and accumulated free induction decays were obtained from up to 3000 scans. A spectral width of 25 000 Hz, a memory of 32 K data points, a 2 s interpulse time, and a 80° radio frequency pulse were used. Prior to Fourier transformation, an exponential multiplication was applied resulting in a 100 Hz line broadening. The residual chemical shift anisotropy, $\Delta\sigma$, was measured as 3 times the chemical shift difference between the high-field peak and the position of isotropically moving lipid molecules at 0 ppm (*33*).

RESULTS

Location and Environment of the Peptide in Model Membranes. The spectral characteristics of the peptide are dominated by the single Trp residue. In solution, the peptide had an absorbance maximum at 290 nm and an emission maximum at 352 nm when excited at the absorbance maximum, indicating that the Trp residue of the peptide was in an aqueous environment. It is known that the Trp fluorescence emission increases with the increase in the environment hydrophobicity, and a blue shift of the emission maximum is observed (*31*). In the presence of increasing concentrations of DMPC, the emission maximum of the Trp did not change at all (Figure 2, panel A). However, increasing concentrations of DMPA shifted the emission maximum to about 345 nm (Figure 2, panel A), a wavelength characteristic of Trp in an environment of low dielectric constant. The emission maximum of the Trp residue was found to shift to about 348 nm using DMPC/DMPA/Chol liposomes (molar ratio of 50:35:15) as a model of a more complex membrane (Figure 2, panel A). The shift of about 7 nm for DMPA

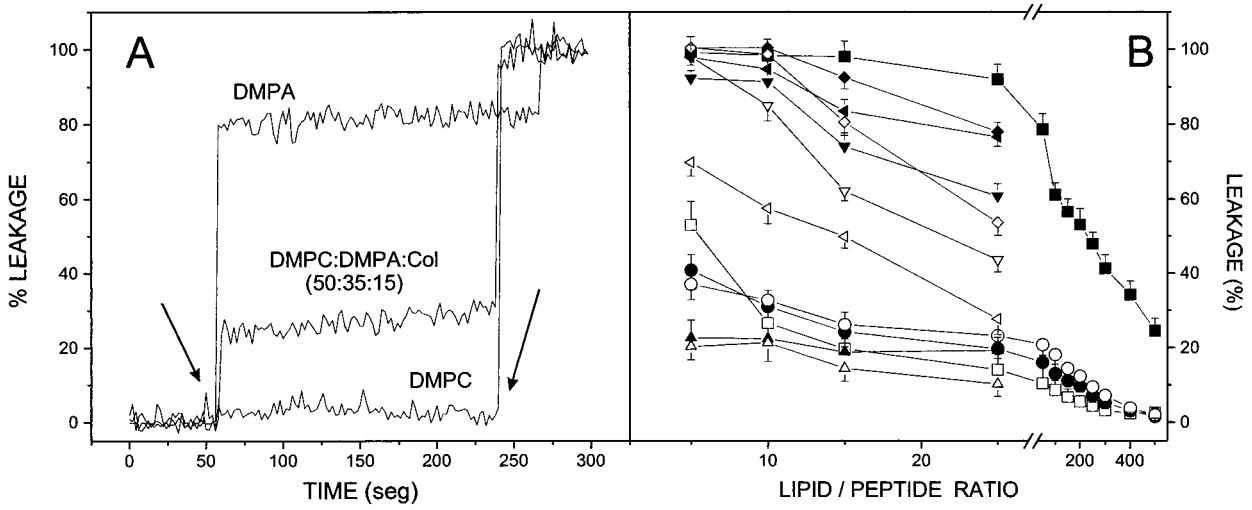

FIGURE 3: Effect of the gp41 fragment on the release of LUV contents for different lipid compositions and different lipid to peptide molar ratios. (A) Representative fluorescence data at 30 °C for three different LUV compositions as indicated. The first arrow indicates the addition of the peptide (final lipid to peptide molar ratio of 50:1, 5:1, and 5:1 for LUV containing DMPA, DMPC, and DMPC/DMPA/Col at a molar ratio of 50:35:15, respectively), whereas the second arrow indicates the addition of Triton X-100. (B) Leakage data for LUV composed of pure DMPA (■, □), pure DMPS (◇, ♦), DMPC/DMPA/Chol at a molar ratio of 50:35:15 (●, ○), DMPC/DMPS/Chol at a molar ratio of 50:35:15 (▲, △), DMPC/DMPS/Col at a molar ratio of 45:45:10 (solid left triangle, open left triangle), and DMPC/DMPS at a molar ratio of 2:1 (▼, ▽). Data were obtained at two different temperatures, 30 °C (closed symbols) and 60 °C (open symbols).

liposomes and about 4 nm for DMPC/DMPA/Chol ones suggests that Trp enters a hydrophobic environment in the presence of liposomes containing DMPA but not in the presence of DMPC liposomes. The peptide, having a theoretical isoelectric point of 8.99, has a charge of about +0.8 at pH 7.4, as used in this work. DMPA, in contrast to the zwitterionic phospholipid DMPC, is a negatively charged phospholipid, so that the binding force of the peptide to liposomes containing DMPA has an apparently electrostatic origin. In these experiments, the phospholipid/peptide molar ratio reaches a very high value (2300:1), and the spectral contribution of free peptide is negligible. The change in the emission maximum wavelength of the Trp has allowed us to obtain the apparent partition coefficient, K_p, of the gp41 fragment. Considering a γ value of 0.519 M^{-1} (*34*), K_p values of $9.3 \pm 3.8 \times 10^4$ and $3.9 \pm 0.6 \times 10^3$ were obtained for liposomes containing DMPA and DMPC/DMPA/Chol (50:35:15), respectively, indicating that the peptide binds to the membrane surface with high affinity. Smaller K_p values have been recently found for the membrane-interacting monomeric form of a related gp41 peptide (residues 579−601) in the presence of phosphatidylglycerol containing model membranes (*13*).

Fluorescence anisotropy measurements can provide very useful insights into the dynamics of the peptide when bound to the membrane. We have obtained the anisotropy values of the gp41 fragment at different lipid/peptide ratios, and the results are shown in Figure 2, panel B. In the presence of DMPC membranes and at all lipid/peptide ratios studied, the anisotropy values for the Trp residue of the peptide remain virtually unchanged presenting a similar value to that found in the aqueous environment. In contrast to the results obtained in the presence of DMPC, we have found that there is an increase of the anisotropy values for the Trp residue of the peptide in the presence of DMPA containing vesicles upon increasing the lipid/peptide ratio (Figure 2, panel B). The limiting value seems to be near 0.10, indicating a significant motional restriction of the Trp moiety of the peptide in the presence of DMPA membranes (*31*).

To investigate the effect of the peptide on the fluidity of the phospholipid model systems, the steady-state emission anisotropy of DPH and TMA-DPH inserted in DMPA multibilayer suspensions in the presence of the gp41 fragment have also been studied. It is generally accepted that DPH has a distribution about a central position in the bilayer (inner probe), whereas its charged derivative TMA-DPH is anchored near the lipid−water interface (interface probe). The gp41 fragment did not change the anisotropy values for both probes inserted in the membrane neither below nor above the phase transition interval, indicating that its location must be at the surface of the membrane (not shown for briefness).

Leakage, Aggregation, and Phospholipid Mixing. To further explore the possible interaction of the gp41 fragment with phospholipid model membranes, we studied the effect of the peptide on the release of encapsulated fluorophores using the experimental set up described in Materials and Methods. Figure 3, panel A, shows the results obtained with three different liposome compositions, namely, DMPA, DMPC, and DMPC/DMPA/Chol at a molar relationship of 50:35:15. It is clearly observed that whereas the peptide hardly exerted any effect on liposomes made of DMPC, it readily interacted with liposomes containing DMPA. Moreover, leakage was dependent on lipid composition as observed in Figure 3, panel A, since leakage was greater for liposomes composed of pure DMPA at a lipid/peptide molar ratio of 50:1 than for liposomes composed of DMPC/DMPA/Chol at a lipid/peptide molar ratio of 5:1, i.e., containing 10 times more peptide than the former one.

Figure 3, panel B, shows the dependence of leakage on the lipid to peptide molar ratio as well as on temperature for different liposome systems. For liposomes composed of pure DMPA and pure DMPS and at 30 °C, i.e., below the gel-to-liquid crystalline transition, leakage increased as the lipid-to-peptide ratio decreased, until a ratio of 15:1 or lower

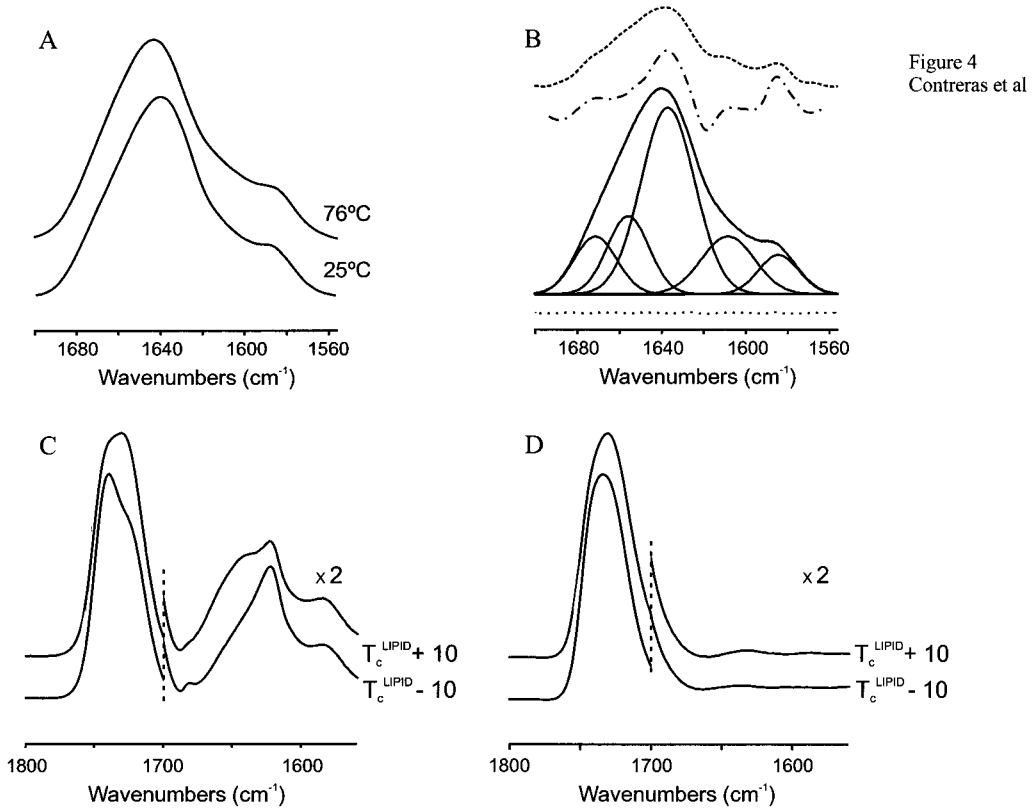

FIGURE 4: (A) Amide I′ band region of the gp41 fragment at 25 and 76 °C as indicated; (B) band decomposition of the amide I′ band region of the gp41 fragment at 25 °C showing the component bands, the fitted envelope, the deconvolved spectrum (- - -), the derivative spectrum (-·-), and the difference between the fitted curve and the original spectrum (·····); and (C, D) the amide I′ and C═O region of the mixture containing the gp41 fragment and either DMPA (C) or DMPC (D) at a phospholipid/peptide molar ratio of 25:1 at two temperatures corresponding to $T_M^{LIPID} \pm 10$ °C.

was reached, were 100% leakage was obtained. Lower leakage values were obtained at 60 °C, i.e., in the liquid crystalline phase, but higher for pure DMPS than for pure DMPA (Figure 3, panel B). Leakage values for samples containing either DMPC/DMPS/Chol or DMPC/DMPA/Chol at a molar ratio of 50:35:15 were significant but lower than for liposomes containing pure DMPS at 30 and 60 °C or liposomes containing pure DMPA at 30 °C; they were similar to the values found for pure DMPA containing liposomes at 60 °C (Figure 3, panel B). Interestingly, liposomes containing significant amounts of DMPS, such as DMPC/DMPS/Chol liposomes at a molar ratio of 45:45:10 or DMPC/DMPS liposomes at a molar ratio of 2:1, showed high leakage values, i.e., a 100% leakage value was obtained at a lipid-to-peptide ratio of 5:1 at 30 °C for both systems (Figure 3, panel B).

We have also studied peptide-induced liposome aggregation and phospholipid mixing using liposomes containing either pure DMPA or DMPC/DMPA/Chol at a relationship of 50:35:15. Liposome aggregation was evident by the increase in light scattering for liposomes containing pure DMPA but only at very low ratios of lipid to peptide, i.e., 5:1 (results not shown). Small values were found for higher lipid-to-peptide ratios and also for DMPC/DMPC/Chol liposomes at all lipid-to-peptide ratios used. The same trend was obtained for phospholipid mixing, since only liposomes containing pure DMPA showed a definite but small increase in the fluorescence signal (less than 3−4%) at a lipid-to-peptide ratio of 5:1, with no effect either at higher ratios or with liposomes containing DMPC/DMPA/Chol (not shown for briefness).

Peptide Structure and Phospholipid Binding. The infrared spectra of the amide I′ region of the fully hydrated peptide in D_2O buffer at 25 and 76 °C and at pH 7.4 are shown in Figure 4, panel A. The spectra are formed by different underlying components that give place to a broad and asymmetric band with a maximum at about 1639 and 1642 cm^{-1} for the spectra at 25 and 76 °C, respectively. Protein denaturation is characterized in D_2O medium by the appearance of two sharp bands at approximately 1685 and 1620 cm^{-1}, due to extended β-strands with strong intermolecular interactions (*35*) that are not observed in the temperature range studied (Figure 4, panel A). If aggregation occurred, it was only to a very low extent.

To observe the underlying components of the broad amide I′ band, we have applied several enhancements methods such as self-deconvolution and derivative methods to the original envelope (*27*) identifying different component bands at frequencies of about 1671, 1654, 1637, 1609, and 1585 cm^{-1}, being the 1637 cm^{-1} band the main one (Figure 4, panel B). To assign the component bands to specific structural features and estimate the percentage of each component, we have decomposed the amide I′ infrared band as described in Material and Methods and the results are also shown in Figure 4, panel B, whereas the values obtained from the fitting are listed in Table 1. Bands appearing at about 1637−1634 cm^{-1} are characteristic of β-sheet structure, whereas component bands at about 1670 and 1690 cm^{-1} are assigned

Table 1: Band Position (cm^{-1}) and Percentage Area (%) Corresponding to the Components Obtained after Curve Fitting the Amide I′ Band of the gp41 Fragment[a]

peptide in solution		peptide plus DMPA[b]			
band position	band area 25 °C	band position	band area 25 °C	band area 56 °C	band area 72 °C
1682		1682	<1		
1671	16	1671			
1656	21	1659	13	33	11
1637	64	1639	39	44	19
1622		1622	48	23	69

[a] The values are rounded off to the nearest integer. [b] DMPA/peptide molar ratio of 25:1.

to β-turns. Bands located at about 1657 cm^{-1} are usually observed for α-helix in D_2O solution, and bands appearing at about 1644−1642 cm^{-1} are assigned in D_2O to unordered structures (*35*). The bands appearing at 1609 and 1585 cm^{-1} are outside the range of frequencies usually observed for the secondary structure elements of proteins (*35*). If we assume that the band at 1671 cm^{-1} is due to β-turns, the band at 1656 cm^{-1} to α-helix and the band at 1637 cm^{-1} to β-sheet, then the gp41 fragment in solution has about 16% of β-turns, 21% of α-helix, and 64% of β-sheet.

Since the COO^- band of DMPS is found around 1622 cm^{-1}, and therefore it might interfere with the amide I′ band of the peptide (*36*), we have studied by infrared spectroscopy the interaction of the peptide with DMPA containing liposomes. To study the peptide when it was effectively bound to the phospholipid membrane, all samples containing both phospholipid and peptide have been prepared by mixing and washing the unbound peptide as described in Materials and Methods. The infrared spectra in the amide I′ and C═O region of samples prepared in this way and containing the peptide and either DMPA or DMPC are shown in Figure 4, panels C and D, respectively. It can be clearly observed that only the amide I′ band corresponding to the bound peptide was present in model membranes composed of DMPA, whereas it was nearly absent in membranes formed by DMPC. When DMPC was used, the peptide was recovered almost completely in the supernatant (not shown), demonstrating therefore that the peptide only binds to negatively charged membranes. Significantly, the amide I′ band envelope of the peptide bound to DMPA is different to that found for the pure peptide in solution (compare the amide I′ region in Figure 4, panels A and C), and therefore, the secondary structure of the bound peptide must be different to that in solution. It is also worth to note that, as shown in Figure 4, panel C, the amide I′ region of the peptide taken at temperatures above and below the main phase transition temperature of the phospholipid were different. These data suggest that the gp41 fragment has a different and distinct conformation when in different phospholipid phases. This is in contrast with the results found with the peptide in solution, where no significant differences were found at all temperatures studied, even at the highest tested (Figure 4, panel A).

Modulation of Phospholipid Phase Behavior. We have studied by infrared spectroscopy the effects of the gp41 fragment on the phase transition of DMPA (the binding to DMPC membranes was negligible and no effect was observed on this phospholipid), which become clearly altered

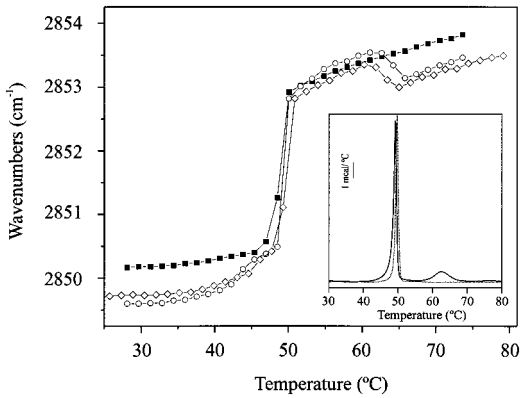

FIGURE 5: Temperature dependence of the CH_2 symmetric stretching band frequency of DMPA for pure DMPA (■) and for samples containing DMPA and the gp41 fragment at a phospholipid/peptide molar ratio of 25:1 (○) and 10:1 (◊). The insert shows the calorimetric traces for pure DMPA (···) and DMPA plus the gp41 fragment at a phospholipid/peptide molar ratio of 25:1 (—).

by the presence of the peptide (Figure 5). It is well established that a shift in the frequency of the CH_2 symmetric stretching band is a reliable index of the phase behavior of a phospholipid dispersion, since the CH_2 stretching frequencies respond primarily to conformational disorder and increase with the introduction of gauche bonds in the fatty acyl chains (*37*). The temperature dependence of the CH_2 symmetric frequency of pure DMPA is shown in Figure 5, where a highly cooperative change at approximately 48 °C is observed, corresponding to the gel-to-liquid crystalline phase transition of the phospholipid. In the presence of the peptide, and in contrast to the pure phospholipid, a decrease in the frequency was observed at temperatures below the gel-to-liquid crystalline phase transition of DMPA (Figure 5), indicating that the proportion of trans isomers was higher in the DMPA/peptide sample than in pure DMPA, and therefore the hydrocarbon chains of DMPA below the main phase transition were more ordered in the presence of the peptide. At temperatures higher than the gel-to-liquid crystalline transition of the phospholipid, a new transition, less cooperative than the main phase transition and characterized by lower frequencies, was observed. This new transition was observed at approximately 62 and 64 °C at phospholipid/peptide molar ratios of 25:1 and 10:1, respectively (Figure 5). In the presence of the peptide it was also possible to observe a small increase in the frequency at about 43 °C that was absent in the pure phospholipid (Figure 5). We have also studied the peptide-induced membrane perturbations on DMPA by differential scanning calorimetry (insert, Figure 5). At a phospholipid/peptide ratio of 25:1, it is possible to observe a cooperative transition at approximately 49 °C, which corresponds to the gel-to-liquid-crystalline ($L_\beta \rightarrow L_\alpha$) phase transition in the lamellar phase, but, significantly, a new broad peak was apparent at temperatures about 62 °C. This new calorimetric peak coincides with the smaller transition observed by infrared spectroscopy (Figure 5).

It is now generally accepted that the *sn-1* and *sn-2* groups of diacylphospholipids, including phosphatidic acid, may be found in lipid vesicles in hydrated and dehydrated states, the proportion of hydrated and dehydrated groups depending on the physical state of the phospholipid bilayer (*38*). Pure DMPA showed a broad C═O carbonyl band that presented after deconvolution two components at 1742 and 1727 cm^{-1}

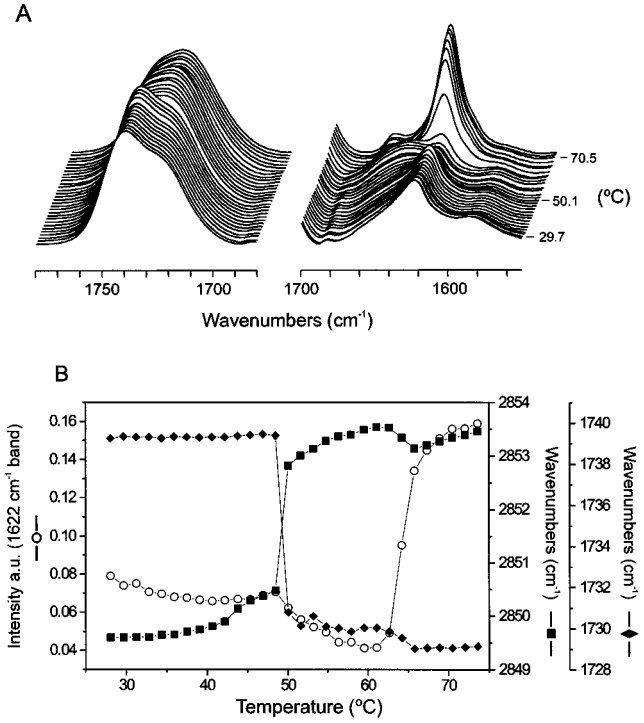

FIGURE 6: (A) Stacked infrared spectra of the C═O and amide I′ regions of the mixture DMPA plus gp41 peptide at a phospholipid/peptide molar ratio of 25:1, recorded at regularly increasing temperature intervals as indicated. (B) Temperature dependence of the CH_2 symmetric stretching (■) and C═O maximum (♦) band frequencies of DMPA and of the intensity of the 1622 cm^{-1} band (○) of the peptide in the mixture DMPA plus gp41 peptide at a phospholipid/peptide molar ratio of 25:1.

(not shown) attributed to dehydrated and hydrated C═O groups, respectively (*36*). The frequencies of these two components were not affected by temperature, but their relative intensities changed as reported for other phospholipids (*37*). Whereas below the phase transition the 1742 cm^{-1} component had a higher intensity than the 1727 cm^{-1} component, at temperatures above the phase transition just the opposite was observed. For pure DMPA, the frequency at the maximum of the C═O vibration band presented one transition at approximately 49 °C (not shown). In the presence of the gp41 fragment, the two components of the C═O carbonyl band did not change in frequency when compared to pure DMPA, but the frequency at the maximum of the C═O vibration band presented two transitions at approximately 49 and 63 °C, in agreement with the transitions previously described (Figure 6, panels A and B).

We have studied other phospholipid bands such as the acyl chain CH_2 scissoring and the PO_2^- double bond stretching bands appearing at 1468 and 1220 cm^{-1}. The presence of the gp41 fragment did not induce any significant differences on frequency and width of these bands when compared with the pure phospholipid, indicating that there were no differences in packing and hydration between the pure phospholipid and the mixtures containing the peptide (not shown).

Secondary Structure of the gp41 Peptide in the Presence of Phospholipid. The temperature dependence of the amide I′ band of the gp41 fragment when bound to DMPA is presented in the stacked plot of the carbonyl and amide I′ regions shown in Figure 6, panel A. It is possible to distinguish two transitions, i.e., the change in the intensity

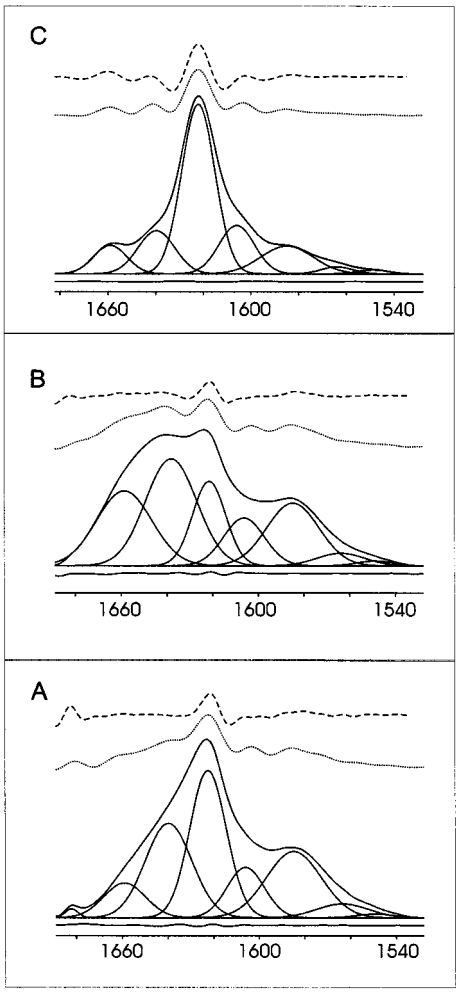

FIGURE 7: Amide I′ band decomposition of the gp41 fragment spectra in the presence of DMPA at a phospholipid/peptide molar ratio of 25:1 in D_2O media at (A) 25, (B) 56, and (C) 72 °C. The component bands, the envelope, the deconvolved (•••) and derivative (---) spectra, and the difference between the fitted curve and the original spectrum are shown.

of the 1622 cm^{-1} band with temperature, which coincides with the transitions observed at 49 and 63 °C in the phospholipid (Figure 6, panels A and B). These two transitions define the boundary for three different amide I′ band envelopes, and therefore three different secondary structures of the gp41 peptide are found corresponding to the different phase states of the phospholipid. Consequently, the secondary structure of the gp41 fragment depends on the phase behavior of the phospholipid molecule, which is in turn modulated by the peptide. The results of the decomposition of the amide I′ of the gp41 fragment in the three different conformations are shown in Figure 7, where it is possible to distinguish different component bands. By observing the derivative and deconvolved spectra, it can be appreciated the existence of several bands displaying different intensities with frequencies at approximately 1682, 1659, 1639, 1622, 1606, 1585, 1564, and 1549 cm^{-1}. Bands at frequencies lower than 1630 cm^{-1} but higher than approximately 1618 cm^{-1} were first described for extended chains in polylysine (*39*) and attributed to antiparallel-chain pleated sheet. They were also found in denatured proteins in D_2O buffer (*40*, *41*). In native proteins, they have been attributed to extended configurations with hydrogen-bonding

to other molecular structures (*42*) or even forming β-hairpins (*43*). Bands appearing at about 1622 cm^{-1} have been also assigned to the existence of oligomeric structures (*44*). The band appearing at 1639 cm^{-1} has an unexpectedly high frequency for β-sheet structures, but in D_2O media unordered structures, even flexible loops, appear at about 1646−1642 cm^{-1} and most probably it can be assigned to β-sheet structures (*35*). Significantly, the intensity of the band at 1622 cm^{-1} increases when the peptide is bound to the phospholipid membrane, and it is also dependent on the phase structure of the phospholipid (Table 1). It should be reminded that this band was completely absent in the spectra of the pure peptide in solution, i.e., in the absence of phospholipid (see Figure 4, panel B).

To enhance the spectral resolution of the amide I′ region of the gp41 fragment in the presence of DMPA model membranes, we have used two-dimensional (2D) correlation spectroscopy to obtain synchronous (synthermal) and asynchronous (asynthermal) spectra, an experimental approach based on the detection of dynamical spectral variations induced by an external perturbation, temperature in our case (*45*). According to the generalized mathematical formalism, synchronous spectra give autopeaks and cross-peaks, located at diagonal and off-diagonal positions. Cross-peaks represent the coincidental changes of spectral signals at two different wavenumbers and suggest the possible existence of a coupled or related origin of the thermally induced spectral intensity variation. Cross-peaks can be positive for bands increasing or decreasing simultaneously and negative for bands that vary in opposite directions (*45*). However, asynchronous spectra contain only cross-peaks characteristic of out-of-phase vibrations. We have used a simplified computational procedure to obtain an approximation to the synchronous and asynchronous (disrelation) spectra (*30*) and are shown in Figure 8. Since we observe simultaneous changes in both peptide and phospholipid infrared bands in the same spectra at the same time, we can correlate coupled changes in specific phospholipid or peptide infrared bands.

The synchronous map obtained for the temperature range between 25 and 56 °C, where the phospholipid main transition is found, is characterized by several correlation peaks (Figure 8, panel A). As the temperature range observed encompasses the phospholipid main transition, several correlation peaks are observed for the phospholipid bands which belong to the CH_2 scissoring (1468 cm^{-1}), C═O carbonyl stretching (1727/1739 cm^{-1}), and CH_2 symmetric and asymmetric stretching bands (2852 and 2918 cm^{-1}, respectively). These correlation cross-peaks are the main ones. On the contrary, cross-peaks that appear in the amide I′ region correlating the peptide bands are very weak, those at 1622/1582 cm^{-1} (positive) and 1660/1622 cm^{-1} (negative), see Figure 8, panel A. These frequencies correspond to the main infrared bands observed in the infrared spectra of the peptide in the presence of the phospholipid. Different cross-peaks correlating phospholipid/peptide bands are also observed, but their intensity is weak (i.e., cross-peaks correlating frequencies at 1622 and 1660 cm^{-1} with the scissoring, carbonyl and CH_2 stretching bands; see Figure 8, panel A). These results show that the main event which takes place at this temperature range is that produced on the phospholipid bands due the phospholipid main transition occurring at 49 °C, there is not an extensive change in conformation for the peptide bands, but the peptide senses the phospholipid phase transition since, as we have shown above, it is bound at the surface of the membrane.

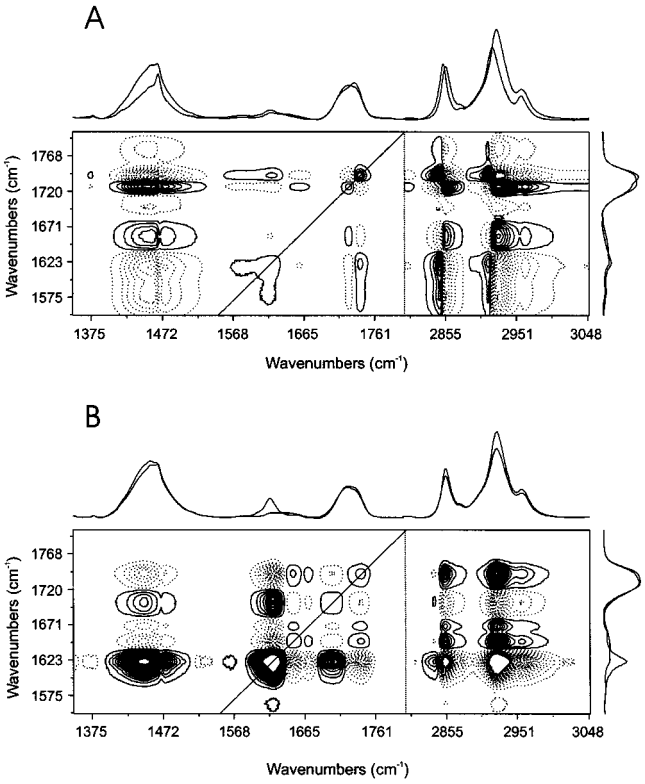

FIGURE 8: Two-dimensional synchronous spectra in the scissoring, amide I′ and CH_2/CH_3 stretching regions for the sample containing DMPA and the gp41 fragment at a phospholipid/peptide molar ratio of 25:1 taken over the range from 25 to 56 °C (A) and from 56 to 74 °C (B). Continuous and dashed lines represent positive and negative peaks, respectively.

The synchronous map obtained for spectra encompassing the temperature range between 56 and 74 °C, where the new 62 °C transition appears, is characterized by one intense and narrow auto-peak at 1620 cm^{-1} (Figure 8, panel B). Several correlation peaks are observed for the phospholipid bands, i.e., CH_2 scissoring (1468 cm^{-1}), C═O carbonyl stretching (1727/1739 cm^{-1}), and CH_2 symmetric and asymmetric stretching bands (2852 and 2918 cm^{-1}, respectively), but they are not so intense as those found for the temperature range where the main transition occurs. Contrary to what was found before, cross-peaks correlating peptide bands and appearing in the amide I′ region are very intense, significantly those correlating the peptide bands appearing at frequencies 1622/1639 cm^{-1} and 1622/1669 cm^{-1} (both of them negative) and 1639/1669 cm^{-1} (positive) (Figure 8, panel B). Several intense cross-peaks correlating phospholipid/peptide bands are also observed, i.e., cross-peaks correlating frequencies at 1622 and 1660 cm^{-1} (weaker) with the scissoring and CH_2 stretching bands (Figure 8, panel B). The disrelation spectra obtained for the same temperature range shows an intense out-of-phase peak at 1622/1639 cm^{-1} indicating that the 1622 and 1639 cm^{-1} bands belong to different conformations.

Effect of the gp41 Fragment on the Polymorphism of DMPA. It is well-known that dispersions of phospholipids, either of biological or synthetic origin, can adopt different structures (micelles, bilayers, hexagonal-H_{II} phases, lipidic particles); such lipid polymorphism can greatly affect the

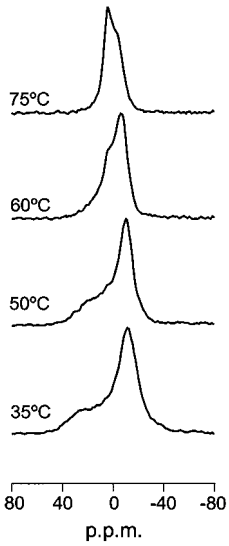

FIGURE 9: ^{31}P NMR spectra of DMPA multilamellar vesicles in the presence of the gp41 fragment at different temperatures as shown. The lipid/peptide ratio was 25:1 and the spectra have been normalized.

functional behavior of membranes (*46*). To discern if the gp41 fragment could affect the phase behavior of DMPA, we have carried out ^{31}P NMR measurements at different temperatures. ^{31}P NMR is sensitive to the motional properties of membrane phospholipids such as local motion and orientation of the phosphate group. In addition, the macroscopic environment of the whole molecule determines the line shape of the ^{31}P NMR resonance spectrum (*47*). This phase sensitivity makes ^{31}P NMR a very suitable tool to follow the structural transitions, if any, in biological and model membranes. Pure DMPA, when organized in bilayer structures, gives rise to an asymmetrical ^{31}P NMR line-shape with a high-field peak and a low-field shoulder, presenting a residual chemical shift anisotropy, $\Delta\sigma$, of approximately 36 ppm in the gel state and approximately 27 ppm in the liquid-crystalline state (not shown for briefness) in agreement with previously published data (*48*). The incorporation of the gp41 fragment in DMPA vesicles at a lipid/peptide ratio of 25:1 did not induce any significant change in the line shape of the ^{31}P NMR spectra at temperatures below the gel-to-liquid crystalline phase transition (Figure 9) when compared to pure DMPA (not shown for briefness). At 60 °C, it was possible to observe the appearance of another low-field component, which, at higher temperatures increased in intensity so that the asymmetrical line-shape observed at low temperature had disappeared completely (Figure 9). The chemical shift anisotropy is lower than that found in the pure lipid in the liquid-crystalline phase, indicating an increase in motional freedom of either the glycerol backbone or the whole molecule (*49*). The chemical shift of this component, approximately 6 ppm, and the reverse symmetry that the line-shape presents, i.e., a low-field peak and a high-field shoulder, similar to that found in membranes presenting the hexagonal H_{II} phase, indicates quite likely that another phase, similar to a H_{II} hexagonal-phase, is induced by the presence of the peptide. The appearance of another phase at high temperatures is in agreement with the change in the CH_2 and C═O stretching frequencies found by infrared and the small low-enthalpy transition found by calorimetry (Figures 5 and 6).

DISCUSSION

Numerous studies have led to the proposal that viral membrane fusion proteins can exist in two major conformations, the native, metastable conformation and the stable, fusogenic conformation (*50*). Understanding the factors that may determine the specificity and stability of these different conformations are therefore required for the understanding of the mechanism of viral entry into cells. The native state of the HIV-1 envelope protein complex is also thought to be metastable, and recent findings suggest that the gp41 ectodomain gives place to different structural changes by a complex series of protein/protein and protein/phospholipid interactions resulting in the co-localization of the virus and cell membranes (*51*). Little is known about how this membrane apposition overcomes the energy barrier for membrane fusion and, moreover, biochemical evidence suggests that more than the N-terminal fusion peptide of gp41 can interact and bind to membranes playing a critical role in membrane apposition and fusion (*13*, *14*).

The interaction of peptides with membrane surfaces involves a number of steps, including the initial binding to the surface, induction or stabilization of a specific secondary structure upon the interaction of the peptide with the phospholipid, modulation of the phospholipid biophysical properties by the peptide binding, and finally insertion of the peptide in the membrane either partially or fully. The 19-amino acid-long peptide from the gp41 ectodomain, subject of this work, binds exclusively and with high affinity to negatively charged membranes, being the binding force apparently of electrostatic origin. This result was already expected due to the positive net charge of the peptide. After binding, the Trp residue resides in an environment of low dielectric constant showing a significant motional restriction, confirming that this portion of the peptide enters a hydrophobic environment but remains located at the surface of the membrane, as indicated by the absence of any effect on the fluorescence anisotropy of both inner and interface probes. This motionally restricted environment is consistent with a location in a region near the membrane interface possibly involved in charge interactions and hydrogen bonding (*13*). The binding of the peptide to negatively charged membranes but not to zwitterionic ones was confirmed also by infrared since only the amide I′ band corresponding to the bound peptide was present in model membranes composed of DMPA, being absent in membranes formed by DMPC.

The infrared spectrum of the amide I′ region of the fully hydrated peptide in D_2O buffer at 25 and 76 °C are very similar, indicating the stability of its conformation in solution, even at high temperatures. When the peptide is bound to the phospholipid, its conformation changes significantly. In the presence of DMPA, a phospholipid that increases significantly the electrostatic component of the peptide partition constant and therefore might stabilize a specific peptide structure upon membrane incorporation (*52*), three different secondary structures of the gp41 peptide are found depending on the phase state of the phospholipid, which on the other hand presents two defined transitions in the presence of the peptide. The 2D-IR results clearly show that the main event that takes place between 25 and 56 °C corresponds to the main phospholipid phase transition, while

the observed changes between 56 and 74 °C correspond to both the phospholipid and the peptide, implying that the new observed transition on the phospholipid involves both types of molecules, peptide and phospholipid. It has been shown that complexes of divalent cations and phosphatidic acid adopt a difference phase at intermediate temperatures that resembles the H_{II} phase (*53*), being suggested to be equivalent to the phase formed during fusion. It is also interesting to note that a transition have been described for phosphatidic acid in the presence of calcium ions and at low pH between 63 and 66 °C (*54*). By using X-ray diffraction, these authors described the appearance of different transitions in this system, which have been ascribed to a rearrangement of hydrocarbon chain packing of the phospholipids from an onthorrombic to a hexagonal lattice (*54*).

Membrane fusion is an energy costing event, since it involves destabilization of the bilayers and dehydration of the interface regions of merging membranes (*55*). Most ambiguity in fusion mechanisms concerns the exact nature of the intermediate state and the molecular arrangements that are involved in the process. The formation of stable oligomers is apparently critical in merging the phospholipids of the two opposing membranes (*56*). Recently, it has been shown that the monomeric form of the gp41 fragment comprising residues 579−601 interacts with negatively charged vesicles, whereas the dimeric form did not (*13*), indicating that differences in the interaction with membranes between monomers and dimers (oligomers) might be important for the viral fusion mechanism. The intensity of the 1622 cm^{-1} band, which could be tentatively assigned to oligomeric structures (*44*), was very small when the peptide was in solution, but it increased in the presence of the negatively charged phospholipid. However, the increase was only significant when the phospholipid changed to this new, H_{II}-like, phase. The location of the peptide at the surface of the membrane could effectively reduce the headgroup area of the phospholipid and promote the formation of the hexagonal-H_{II}-like phase. Although we have used model membranes composed of DMPA, which is not representative of the cellular plasma membrane, the structural changes that take place when the peptide binds to the membrane, could be indicative of the conformational change that takes place during the native (metastable) to fusogenic (stable) conformational change of gp41 following binding of the HIV-1 envelope glycoprotein to its receptors. Indeed, leakage of vesicular contents is observed either in the presence of DMPA-containing liposomes or in the presence of DMPS-containing liposomes, with or without cholesterol. The change in conformation and the possible formation of oligomeric forms in the presence of the membrane could indicate the propensity of the peptide to self-assemble and suggests that these changes are part of the structural transition that transform gp41 from the fusion-inactive to the fusion-active state, being most probably the dominant form during membrane fusion. For example, induced oligomerization of protein A/gp41$^{538-593}$ and maltose-binding protein/gp41$^{558-595}$ chimeric proteins have been described (*57*, *58*). The zipper-like domain of gp41 comprising residues 555−583 (recall that the gp41 fragment we are studying here encompasses residues 579−597) seems to be the responsible for this induced oligomerization, since the native proteins are monomeric (*57*, *58*).

It has been shown that the peptide corresponding to the hydrophobic NH_2-terminal fusion domain of gp41 is sufficient to cause leakage and phospholipid mixing in vesicles (*16*); similar effects have been described in this work for the 579−597 peptide. It is then possible that the core oligomeric complex formed by the zipper-like coiled-coil and COOH-terminal helices of the gp41 ectodomain acts as a joint to hold the oligomeric structure, while the fusion domain bring the two opposing membranes into contact. The peptide we have studied in this work is also capable of binding and modifying the biophysical properties of phospholipid model membranes, a property that could provide an additional driving force for the merging of the two viral and target cell membranes. Tendency to oligomerize and membrane binding can exert an additional force promoting membrane coalescence. It should be recalled that the fusion peptide of the gp41 ectodomain is not likely to be completely exposed to the solvent because of its hydrophobicity and therefore must be guided to the target membrane by other components during the fusion process. Membrane fusion and the lamellar-to-hexagonal phase transition have been suggested to be linked via common intermediating structures (*59*). Inverted hexagonal H_{II}-phase forming lipids, such as diacylglycerols or phosphatidylethanolamines, promote fusion when introduced into bilayers composed of lipids forming lamellar phases, but micelle-forming lipids, such as lysophosphatidylcholines, inhibit fusion (*60*). Since the gp41 peptide fragment we have studied here is capable of inducing a H_{II}-like phase, it would be tempting to speculate that the region where the sequence resides in the native protein plays a significant role in the fusion mechanism induced by gp41.

In conclusion, the results shown here, i.e., the gp41$^{579-597}$ sequence binds and interact with negatively charged phospholipids, its conformation is significantly different in a membraneous environment, the propensity to change the phase structure of the membrane, complement the structural investigations of the different domains of the gp41 protein, the zipper-like domain, the COOH-terminal helix and the NH_2-terminal fusion domains and our findings argue in favor of its direct role in the fusion reaction mediated by HIV. Similar mechanisms might be used by other enveloped viruses in mediating virus-target cell fusion.

ACKNOWLEDGMENT

We thank Dr. R. Mateo for her help on the fluorescence measurements, and Prof. E. Villar and Dr. V. Shnyrov for their helpful discussions. L.M.C. is a recipient of a predoctoral fellowship from the “Consejo Nacional de Investigaciones Científicas y Tecnológicas”, CONICIT, Venezuela.

REFERENCES

1. Turner, B. G., and Summers, M. F. (1999) *J. Mol. Biol. 285*, 1−32.
2. Wild, C., Oas, T., McDanal, C., Bolognesi, D., and Matthews, T. (1992) *Proc. Natl. Acad. Sci. U.S.A. 89*, 10537−10541.
3. Chan, D. C., and Kim, P. S. (1998) *Cell 93*, 681−684.
4. Ferrer, M., Kapor, T. M., Strausmaier, T., Weissenhorn, W., Skehel, J. J., Oprian, D., Schreider, S. L., Wiley, D. C.; Harrison, S. C. (1999) *Nat. Struct. Biol. 6*, 953−960.
5. Neurath, A. R., Strick, N., and Jiang, S. (1992) *Virology 188*, 1−13.

6. Chan, D. C., Fass, D., Berger, J. M., and Kim, P. S. (1997) *Cell 89*, 263−273.
7. Weissenhorn, W., Dessen, A., Harrison, S. C., Skehel, J. J., and Wiley, D. C. (1997) *Nature* 387, 426−430.
8. Lu, M., Blacklow, S. C., and Kim, P. S. (1995) *Nat. Struct. Biol. 2*, 1075−1082.
9. Bentz, J. (2000) *Biophys. J. 78*, 886−900.
10. Epand, R. M., and Epand, R. F. (1994) *Biochem. Biophys. Res. Commun. 202*, 1420−1425.
11. Gray, C., Tatuliam, S. A., Wharton, W. A., and Tamm, L. K. (1996) *Biophys. J. 70*, 2275−2286.
12. Pritsker, M., Jones, P., Blumenthal, R., and Shai, Y. (1998) *Proc. Natl. Acad. Sci. U.S.A. 95*, 7287−7292.
13. Santos, N. C., Prieto, M., and Castanho, A. R. B. (1998) *Biochemistry 37*, 8674−82.
14. Shu, W., Ji, H., and Lu, M. (2000) *J. Biol. Chem. 275*, 1839−1845.
15. Rapaport, D., and Shai, Y. (1994) *J. Biol. Chem. 269*, 15124−15131.
16. Nieva, J. L., Nir, S., Muga, A., Goñi, F. M., and Wilschut, J. (1994) *Biochemistry 33*, 3201−3209.
17. Martin, I., Defrise-Quertain, F., Decroly, E., Vandenbranden, M., Brasseur, R., and Ruysschaert, J. M. (1993) *Biochim. Biophys. Acta 1145*, 124−133.
18. Wang, J. J. G., Steel, S., Wisnielowski, R., and Wang, C. Y. (1986) *Proc. Natl. Acad. Sci. U.S.A. 83*, 6159−6163.
19. Rabenstein, M. D., and Shin, Y. K. (1996) *Biochemistry 35*, 13922−13928.
20. Fernández-Ballester, G., Gavilanes, F., Albar, J. P., Ferragut. J. A., and González-Ros, J. M. (1995) *Biophys. J. 68*, 858−865.
21. Surewicz, W. K., Mantsch, H. H., and Chapman, D. (1993) *Biochemistry 32*, 389−394.
22. Zhang, T. P., Lewis, R. N. A. H., Hodges, R. S., and McElhaney, R. N. (1992) *Biochemistry 31*, 11572−11578.
23. Hope, M. J., Bally, M. B., Webb, G., and Cullis, P. R. (1985) *Biochim. Biophys. Acta 812*, 55−65.
24. Böttcher, C. S. F., Van Gent, and Fries, C. (1961) *Anal. Chim. Acta* 203−204.
25. Edelhoch, H. (1967) *Biochemistry 6*, 1948−1954.
26. Corbalán-García, S., Teruel, J. A., Villalaín, J., and Gómez-Fernández, J. C. (1994) *Biochemistry 33*, 8247−8254.
27. Kauppinen, J. R., Moffatt, D. J., Mantsch, H. H., and Cameron, D. G. (1981) *Appl. Spectrosc. 35*, 271−276.
28. Mantsch, H. H., Moffatt, D. J., and Casal, H. (1988) *J. Mol. Struct. 173*, 285−298.
29. Bañuelos, S., Arrondo, J. L. R., Goñi, F. M., and Pifat, G. (1995) *J. Biol. Chem. 270*, 9192−9196.
30. Burie, J. R. (1996) *Appl. Spectrosc. 50*, 861−865.
31. Lakowicz, J. R. (1999) *Principles of Fluorescence Spectroscopy*, 2nd ed., Plenum Press, New York.
32. Struck, D. K., Hoekstra, D., and Pagano, R. E. (1981) *Biochemistry 20*, 4093−4099.
33. Seelig, J. (1978) *Biochim. Biophys. Acta 515*, 105−140.
34. Marsh, D. (1990) *CRC Handbook of Lipid Bilayers*, CRC Press, Boca Ratón, FL.
35. Arrondo, J. L. R., Muga, A., Castresana, J., and Goñi, F. M. (1993) *Prog. Biophys. Mol. Biol. 59*, 23−56.
36. Martínez-Senac, M., Villalaín, J., and Gómez-Fernández, J. C. (1999) *Eur. J. Biochem. 265*, 744−753.
37. Mantsch, H. H., and McElhaney, E. N. (1991) *Chem. Phys. Lipids 57*, 213−226,
38. Blüme, A., Hübner, W., and Messner, G. (1988) *Biochemistry 27*, 8239−8249.
39. Susi, H. (1969) in *Structure and Stability of Biological Macromolecules* (Timashef, S. N., Stevens, L., Eds.) pp 575−663, Dekker, New York.
40. Muga, A., Arrondo, J. L. R., Bellon, T., Sancho, J., and Bernabeu, C. (1993) *Arch. Biochem. Biophys. 300*, 451−457.
41. Naumann, D., Schultz, C., Gorne-Tschelnokow, U., and Hucho, F. (1993) *Biochemistry 32*, 3162−3168.
42. Arrondo, J. L. R., Young, N. M., and Mantsch, H. H. (1988) *Biochim. Biophys. Acta 952*, 261−268.
43. Chehin, R., Iloro, I., Marcos, M. J., Villar, E., Shnyrov, V. L., and Arrondo, J. L. R. (1999) *Biochemistry 38*, 1525−1530.
44. Chehin, R., Thorolfsson, M., Knappskog, P. M., Matínez, A., Flatmark, T., Arrondo, J. L. R., and Muga, A. (1998) *FEBS Lett. 422*, 225−230.
45. Noda, I. (1993) *Appl. Spectrosc. 47*, 1329−1336.
46. Kruijff, B., Cullis, P. R., Verkleij, A. J., Hope, M. J., Van Echteld, C. J. A., and Taraschi, T. F. (1985) in *The Enzymes of Biological Membranes*, 2nd ed. (Martonosi, A. N., Ed.) Vol. 1, 131−204, Plenum Press, New York.
47. Killian, J. A., Borle, F., De Kruijff, B., and Seelig, J. (1986) *Biochim. Biophys. Acta 854*, 133−142.
48. Pott, T., Mailet, J. C., and Dufourc, E. J. (1995) *Biophys. J. 69*, 1897−1908.
49. Van Echteld, C. J. A., De Kruijff, B., Mandersloot, J. G., and De Gier, J. (1981) *Biochim. Biophys. Acta 649*, 211−220.
50. Carr, C. M., Chaudhry, C., and Kim, P. S. (1997) *Proc. Natl. Acad. Sci. U.S.A. 94*, 14306−14313.
51. Furuta, R. A., Wild, C. T., Weng, Y., and Weiss, C. D. (1998) *Nat. Struct. Biol. 5*, 276−279.
52. Thorgeirsson, T. E., Russell, C. J., King, D. S., and Shin, Y. K. (1996) *Biochemistry 35*, 1803−1809.
53. Miner, V. W., and Prestegard, J. H. (1984) *Biochim. Biophys. Acta 774*, 227−236.
54. Takahashi, H., Yasue, T., Ohki, K., and Hatta, I. (1995) *Biophys. J. 69*, 1464−1472.
55. Rand, R. P. (1981) *Annu. Rev. Biophys. Bioeng. 10*, 277−314.
56. Chang, D. K., Cheng, S. F., and Trivedi, V. D. (1999) *J. Biol. Chem. 274*, 5299−5309.
57. Schugars, D. C., Wild, C. T., Greenwell, T. K., and Mathhews, T. J. (1996) *J. Virol. 70*, 2982−2991.
58. Bernstein, H. B., Tucker, S. P., Kar, S. R., McPherson, S. A., McPherson, D. T., Dubay, J. W., Lebowitz, J., Compans, R. W., and Hunter, E. (1995) *J. Virol. 69*, 2745−2750.
59. Siegel, D. P., and Epand, R. M. (1997) *Biophys. J. 73*, 3089−3111.
60. Chernomordik, L. (1996) *Chem. Phys. Lipids 81*, 203-213.

BI002613U